IEEE Access
Multidisciplinary | Rapid Review | Open Access Journal

Received September 5, 2019, accepted October 15, 2019, date of publication October 28, 2019, date of current version November 7, 2019.

Digital Object Identifier 10.1109/ACCESS.2019.2949795

A 3D-Printed Tapered Cavity-Backed Flush-Mountable Ultra-Wideband Antenna for UAV

SEONGKYU LEE[1], SUNRYUL KIM[1], YOUNGMI PARK[2], AND JAEHOON CHOI[1]
[1]Department of Electronics and Computer Engineering, Hanyang University, Seoul 133-791, South Korea
[2]Electronic Warfare PMO, Agency for Defense Development, Daejeon 305-600, South Korea

Corresponding author: Jaehoon Choi (choijh@hanyang.ac.kr)

This work was supported in part by the Signal Intelligence Research Center supervised by the Defense Acquisition Program Administration, and in part by the Agency for Defense Development of Korea.

ABSTRACT A tapered cavity-backed flush-mountable dual mono-cone antenna is proposed. The proposed antenna consists of four main sections: a lower mono-cone, an upper mono-cone, novel feeding structures, and an exponentially tapered cavity. To obtain high-frequency band operation, the upper mono-cone excited by the feeding structures is located inside the lower mono-cone. The circular cavity used in the proposed antenna has a tapered wall for mitigating the deterioration of radiation performance. The proposed antenna has overall dimensions of 200 mm × 200 mm × 30 mm. The measured reflection coefficients (S-parameters) are below −10 dB from 1.43 GHz to 39.05 GHz (1:27.3). The measured radiation pattern has a quasi-omnidirectional characteristic in the operating frequency band.

INDEX TERMS 3D printed components, UWB antenna, flush-mountable antenna, cavity-backed antenna, UAV.

I. INTRODUCTION

In recent years, unmanned aerial vehicles (UAVs) have been studied for a wide range of applications [1]–[3]. The most common uses for UAVs are surveillance and military applications. The ELINT system collects a wide spectrum of electrical signals (from the VHF band to the Ka band) and locates targets [4]–[6]. To perform such applications successfully, an antenna with an omnidirectional radiation pattern in the horizontal plane and a wide frequency bandwidth is required. In addition, the antenna mounted on the UAV must have a low profile and be lightweight to meet the aerodynamic requirements and satisfy the payload capacity limit. To attain an omnidirectional radiation pattern in the horizontal plane, a blade type antenna has been developed for UAV applications [7]–[9]. In [7], a broadband, slotted blade dipole antenna was proposed. The antenna uses a combination of two vertical tails and two perpendicular slots. It is small and lightweight, and has omnidirectional characteristics in a wide frequency band. In [8], the researchers proposed a tri-band, horizontally-polarized omnidirectional antenna combining a folded tapered patch and a vertical slot together inside the rectangular cavity. A blade type VHF-UHF band antenna for aircraft usage was designed using nth-order polynomial curvature for both the radiation and extended ground to obtain a wide frequency band [9]. However, such antennas can cause drag problems at high speeds and are fragile. To overcome these issues, many studies on low-profile conformal antennas have been conducted [10]–[12]. In [10], the researchers used a planar monopole with shorted pin antenna. It was conformal to the UAV surface to obtain the desired omnidirectional radiation characteristics by inducing a current on the shorted pin. In [11], four horns using SIW technology were integrated on the substrate locating on UAV surface for generating a quasi-omnidirectional radiation pattern in the horizontal plane. In [12], arc-shaped patches and a disk-loaded feeding pin were utilized to obtain omnidirectional radiation with a reduced antenna height. Although these conformal antennas have omnidirectional radiation patterns and are low-profile to alleviate wind influence at high speeds, they have a narrow operating frequency band. To improve the bandwidth performance in low-profile environments, methods for embedding a mono-cone antenna inside a cavity were developed in [13]–[15]. A wideband flush-mountable mono-cone antenna embedded inside a conventional cavity wall was proposed in [13]. In [14], to produce omni-directional

The associate editor coordinating the review of this manuscript and approving it for publication was Diego Masotti.

TABLE 1. Parameter values for the profile of the tapered cavity bottom.

Profile No.	A	B	C	D	x
1	5.6.E-05	70	0	0	$0 \le x \le 80$
2	-2.4.E-02	-50	80	15	$80 \le x \le 100$
3	1.0.E-03	100	0	23	$0 \le x \le 15$
4	-5.5.E-03	-100	20	26.5	$15 \le x \le 30$

radiation and a wide operating frequency band, a rectangular cavity with an inclined wall was used. However, the bandwidth of this type of antenna is not wide enough, due to the effect of resonance occurring in the circular cavity. Therefore, for this study, we located a mono-cone inside an exponentially tapered cavity to reduce the reflection from the cavity wall (which occurred in our previous work [15]).

3D printing technology is an attractive research topics due to its advantages of low cost, lightweight production items, and ease of fabrication. Due to its numerous advantages, many microwave components have been fabricated using 3D printing technology [15]–[18]. Generally, to fabricate a 3D printed antenna, a conductive material needs to be painted on a non-conductive structure made by a 3D printer.

In this paper, we propose a 3D-printed tapered cavity-backed flush-mountable ultra-wideband antenna for UAV applications. The proposed antenna has a novel dual mono-cone structure. The upper mono-cone is embedded inside the top surface of the lower mono-cone to obtain a wide operating frequency band, and a novel shorting structure is utilized for feeding the upper mono-cone. To minimize the weight, the exponentially tapered cavity and the lower mono-cone were fabricated by 3D printing technology. The proposed antenna has an omnidirectional radiation pattern over the ultra-wide frequency band. To verify the performance of the proposed antenna, numerical simulations as well as measurements were performed.

II. ANTENNA DESIGN

A. ANTENNA GEOMETRY

The configuration of an exponentially tapered cavity-backed dual mono-cone antenna is illustrated in Fig. 1. The antenna consists of two mono-cones and shorting structures inside the metal cavity, which has an exponentially tapered wall. The large mono-cone is designed to operate in the lower frequency band, and the small mono-cone embedded into the top surface of the large mono-cone is optimized to operate in the higher frequency band. The large mono-cone is excited by a SMA connector attached to the bottom of the exponentially tapered cavity. A novel coaxial probe with the shape of a helix with a 90-degree turn is used to feed the small mono-cone. The probe penetrates the exponentially tapered cavity and the large mono-cone. The outer conductor of the probe is connected to the ground of the exponentially tapered cavity and the side surface of the large mono-cone. The inner conductor of the probe is directly attached to the small

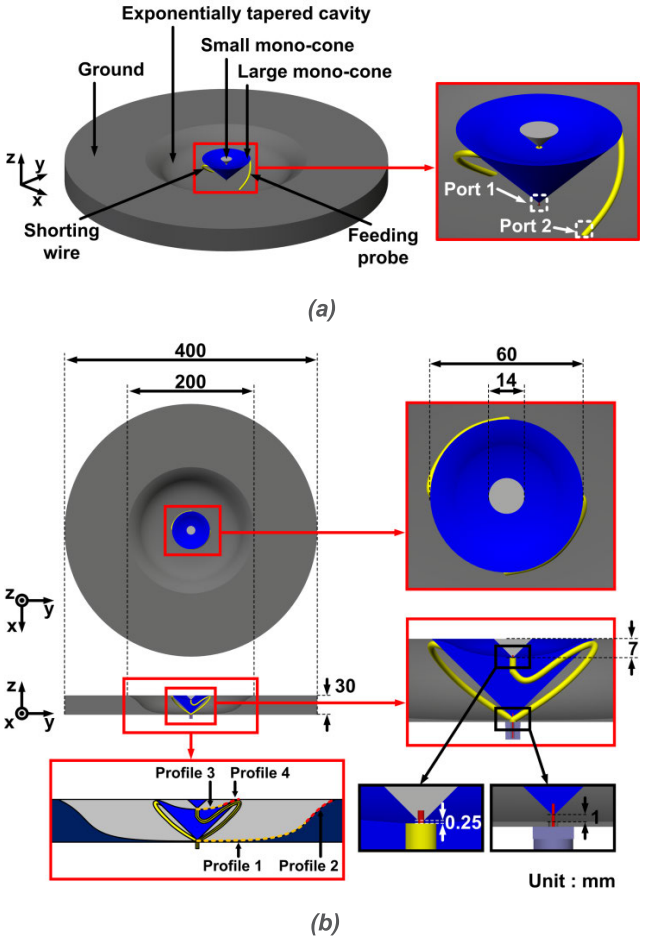

FIGURE 1. Geometry of the proposed antenna: (a) perspective view and (b) top and side views.

mono-cone. A shorting wire having the same shape as the coaxial probe is located on the opposite side of the large mono-cone. The exponentially tapered cavities have dual exponential profiles for enhancing the operation bandwidth [19]–[20]. The parameters for the design of the tapered cavity are denoted in Equation (1), and their corresponding values are provided in Table 1. These values are optimized to provide the best antenna performance. The dimensions of the exponentially tapered cavity-backed dual mono-cone antenna are 200 mm × 200 mm × 30 mm with a circular ground with a diameter of 400 mm, which is useful when considering the aerial fuselage laid outside the antenna.

$$z = A(e^{B(x-C)} - 1) + D \tag{1}$$

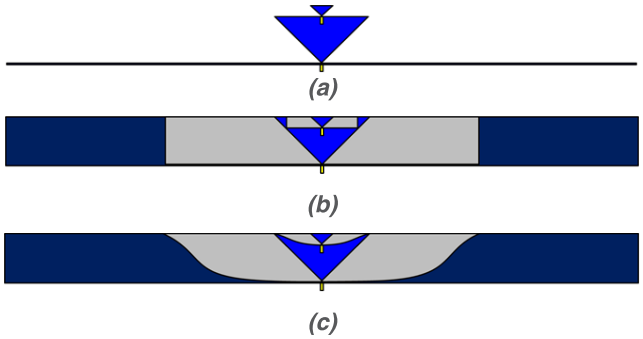

FIGURE 2. The evolution process of the proposed antenna: (a) ANT1, (b) ANT2, and (c) ANT3.

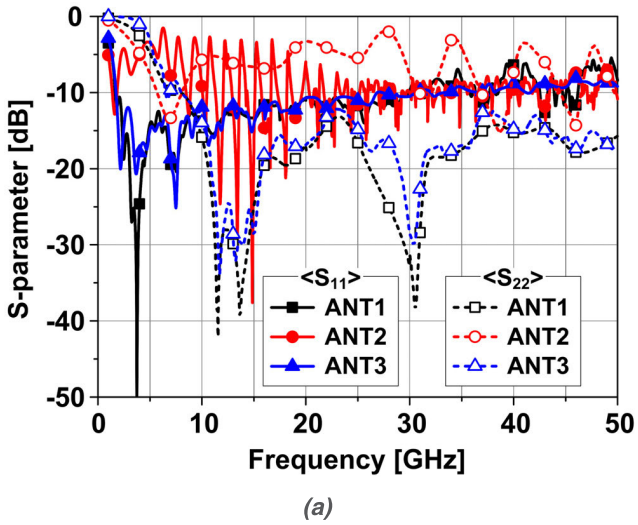

FIGURE 3. Simulated results of ANT1, ANT2, and ANT3: (a) s-parameter and (b) impedance.

B. ANTENNA ELEMENT DESIGN AND ANALYSIS

Fig. 2 illustrates the evolution process of the proposed antenna. The performance of the antenna at each step was simulated by Ansoft HFSS [21]. As shown in Fig. 2 (a), ANT1 is a simple stacked dual mono-cone antenna with a small mono-cone on the top surface of the large mono-cone.

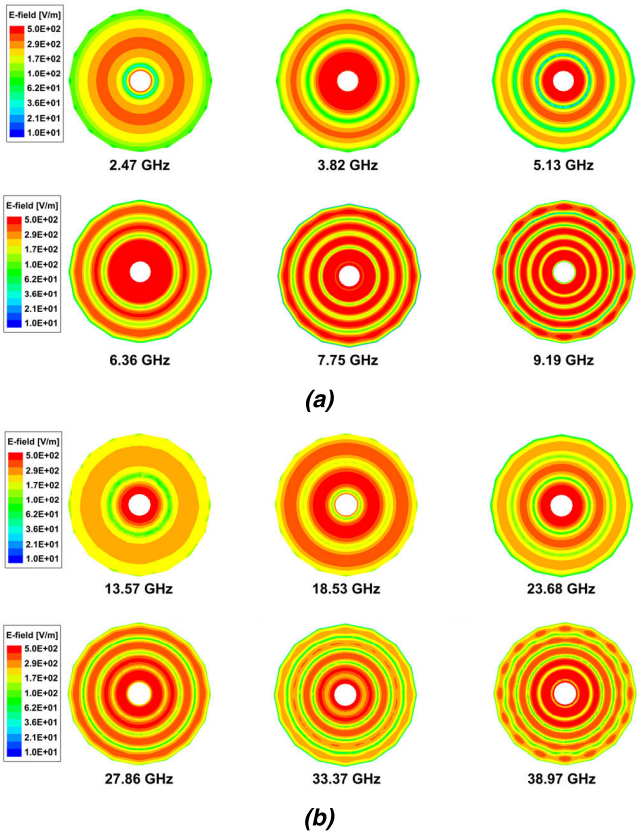

FIGURE 4. Simulated electrical field distribution (xy-plane) of ANT3: (a) inside the large circular cavity and (b) inside the small circular cavity.

The gap between the ground and the large mono-cone is 1 mm and the gap between the small mono-cone and the large mono-cone is 0.25 mm. The heights of the large mono-cone and the small mono-cone are 29 mm and 6.75 mm, respectively. Both mono-cones have a 90-degree flange angle. It is well known that a mono-cone with a 90-degree flange angle provides a wide bandwidth [22]. Figs. 3 (a and b) show that ANT1 has a wide −10 dB bandwidth for the large mono-cone (S_{11}: 1.66 GHz to over 20 GHz) and for the small mono-cone (S_{22}: 8 GHz to over 50 GHz). Although ANT1 has an ultra-wide bandwidth, the antenna height is not suitable for UAV application due to the stacked structure. To ensure the antenna is flush mountable in the flat ground, the top surface of the large mono-cone is excavated. The large circular cavity formed by the excavation has a radius of 100 mm and a depth of 30 mm. The small circular cavity formed inside the large mono-cone has a radius of 22.5 mm and a depth of 7 mm. The large mono-cone and small mono-cone are located inside the cavity. Fig. 2 (b) shows this antenna, referred to as ANT2. Even though ANT2 has a flush-mountable shape, the reflection coefficient characteristic of ANT2 (shown in Fig. 3) is deteriorated, due to the oscillating phenomenon inside the cavity. The magnitude of the antenna impedance increases over time due to the circular cavity. The electromagnetic wave generated by the mono-cone propagates toward the wall of

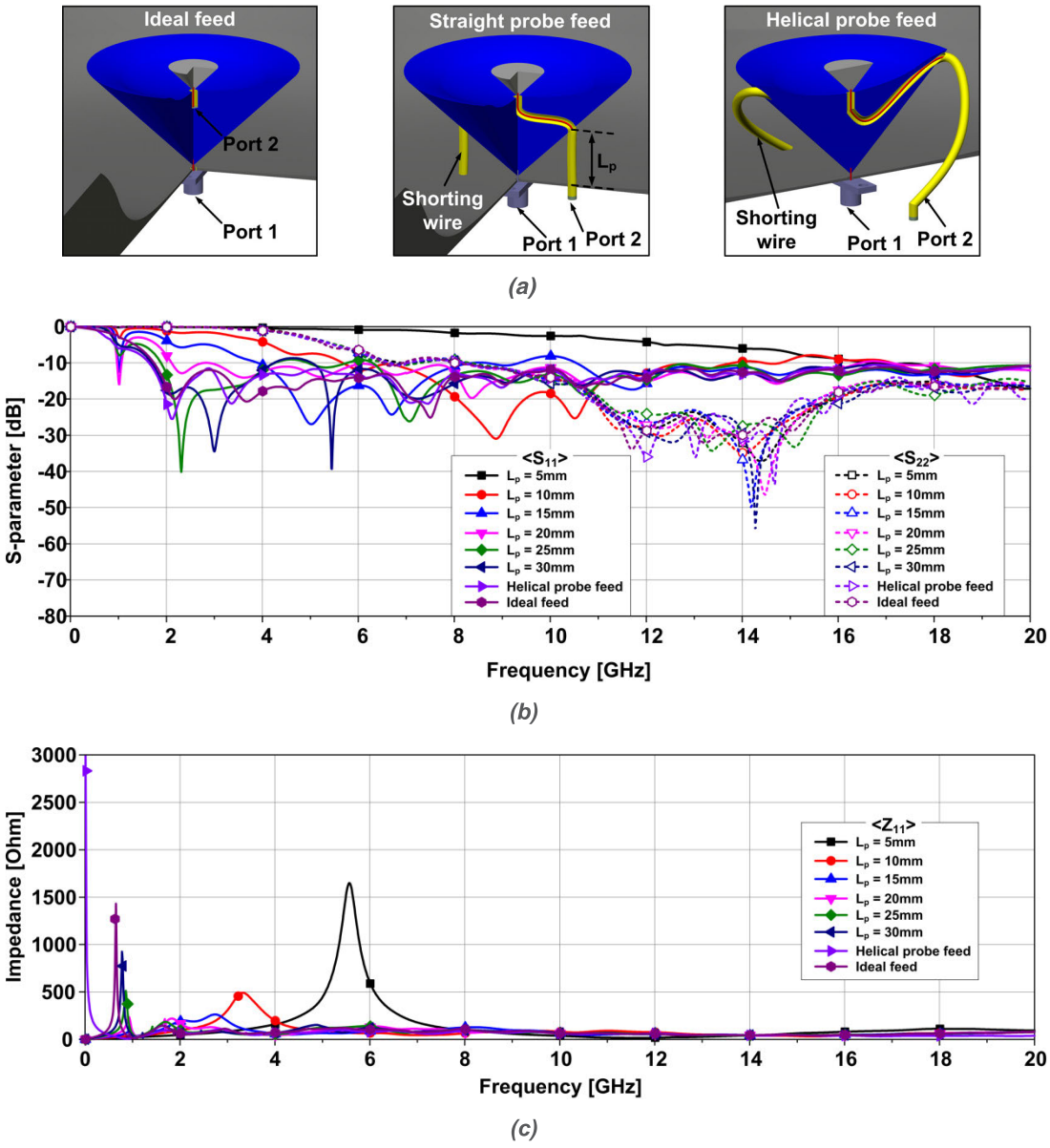

FIGURE 5. Various prototypes of the feeding network: (a) geometry, (b) simulated s-parameter, and (c) simulated impedance.

the circular cavity and a substantial portion of the wave is reflected due to impedance mismatch. In Fig.4 considering the peak impedance values of ANT2, the E-field distributions with respect to the frequencies show that the field strength increases along the radial direction inside the cavities as the frequency increases. To prevent such phenomena in the circular cavities, the walls of the cavities are tapered with an exponential profile. Fig. 2 (c) illustrates an antenna with exponentially tapered cavities (ANT3). Because the tapering profile mitigates the impedance mismatch at the cavity wall, an electromagnetic wave generated inside the exponentially tapered cavities propagates with little reflection at the outer region of the cavity, resulting in a low reflection coefficient of the antenna [8]. Fig. 3 shows that ANT3 has s-parameter and input impedance characteristics similar to those of ANT1 under a flush-mountable environment.

C. ANTENNA FEEDING NETWORK DESIGN AND ANALYSIS

In the design process for ANT3, an ideal feed providing direct excitation to the small mono-cone is assumed. However, it is difficult to realize the ideal feed in a stacked structure. Although a more realistic feeding configuration, such as multi-coaxial feed, can be implemented to excite the stacked structure [23], [24], such a feeding technique has inherent difficulty in reducing the influence of the induced current on the feed cable, which can deteriorate the reflection coefficient of the antenna. Therefore, a novel helical feeding network

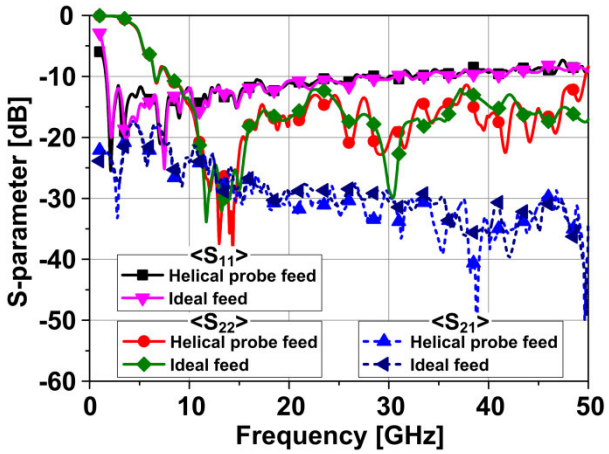

FIGURE 6. Simulated s-parameters of antenna element with ideal feed and helical probe feed.

for the dual mono-cone antenna was designed for achieving a similar performance as that obtained when using the ideal feed. Fig. 5 (a) shows the geometries associated with an ideal feed, a straight probe feed, and a helical probe feed. In the straight probe feed, the feeding probe used to excite the small mono-cone is located off-center to handle the parallel resonance due to the feeding network, and the shorting wire is placed on the opposite side as the feeding probe to balance the radiation pattern of the antenna [25]–[27]. To understand the impact of the feeding line on the antenna performance, antenna elements with various lengths of feeding probe are analyzed. Fig. 5 (b) and (c) show the simulated s-parameter and impedance of antenna elements for ideal feed, helical probe feed, and straight probe feed with various length of feeding probe. When the feeding probe has a length of 5 mm, the parallel resonance occurs at approximately 5.5 GHz, and the S_{11} characteristic is deteriorated. The parallel resonance due to the feeding probe is shifted toward low frequencies as the length of the feeding probe increases. Although the straight feeding line with 30 mm length reduces the influence on the antenna performance, the S_{11} of the antenna element is still affected by the feeding network. To lessen the impact of parallel resonance on antenna operation, a helical feeding network is designed. The feeding network has a helical shape with a 90-degree turn to provide additional length to the feeding probe. Fig. 6 compares the simulated s-parameters of an antenna with an ideal feed and an antenna with a helical probe feed. The simulated results show that the antenna with a helical probe feed performs similarly to the antenna with an ideal feed throughout the entire operating frequency. The simulated -10 dB S_{11} bandwidth of the antenna element with the helical probe feed is 11.32 GHz (1.68 GHz-13 GHz) in the lower band and that of S_{22} is 28.7 GHz (9.3 GHz-38 GHz) in the higher band. The antenna element with the helical feeding network exhibits a good isolation characteristic between Port1 and Port2, taking a value below -15 dB throughout the entire operating frequency band.

D. FABRICATION USING 3D PRINTER

The entire structure was printed by a 3D printer with 0.1 mm resolution. To consider the effect of fuselage of the UAV, a circular ground is attached. Since the printing capacity of a 3D printer is limited, the S-parameters of the exponentially tapered cavity-backed dual mono-cone antenna with various extended circular ground sizes are simulated to determine the minimum ground size necessary to emulate the actual ground of a UAV. Fig. 7 shows that the simulated S_{11} and S_{22} of the antenna are not significantly changed when R_g is greater than 200 mm. Therefore, we printed the antenna with an extended circular ground with a radius of 200 mm.

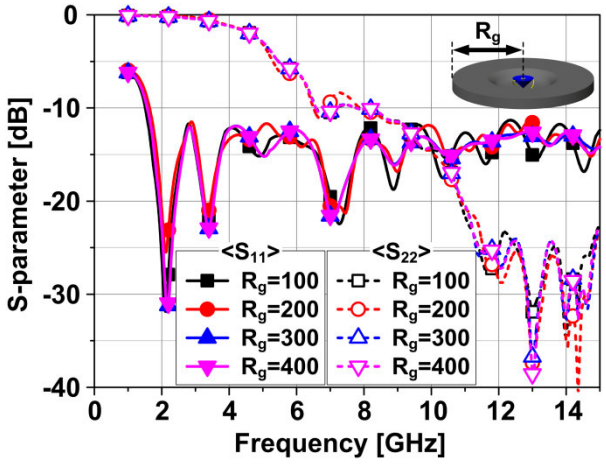

FIGURE 7. Simulated s-parameters of the antenna with extended circular ground.

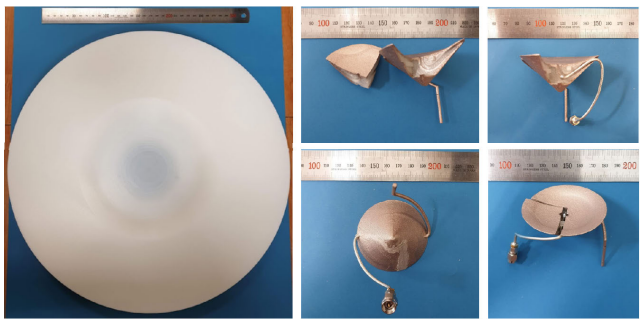

FIGURE 8. Photographs of the printed parts of the antenna: (a) the tapered cavity and (b) the printed mono-cone with feeding structures.

Fig. 8 (a) shows the printed exponentially tapered cavity. The lower mono-cone was split into 2 pieces to enable embedding of the helical probe. They were assembled as shown in Fig. 8 (b). The assembled structure was coated with three layers of conductive paint containing silver particles to produce a conducting surface [15], [16].

III. SIMULATED AND MEASURED RESULTS

Photographs of the exponentially tapered cavity-backed dual mono-cone antenna are shown in Figs. 9(a and b).

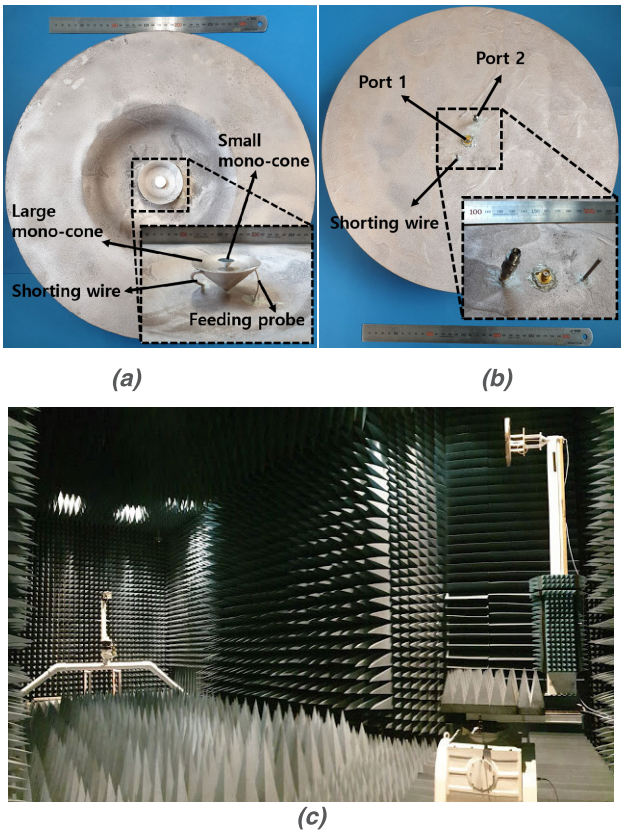

FIGURE 9. Fabrication of the antenna: (a) top view of the fabricated antenna, (b) bottom view of the fabricated antenna, and (c) testing environment for measuring antenna performance.

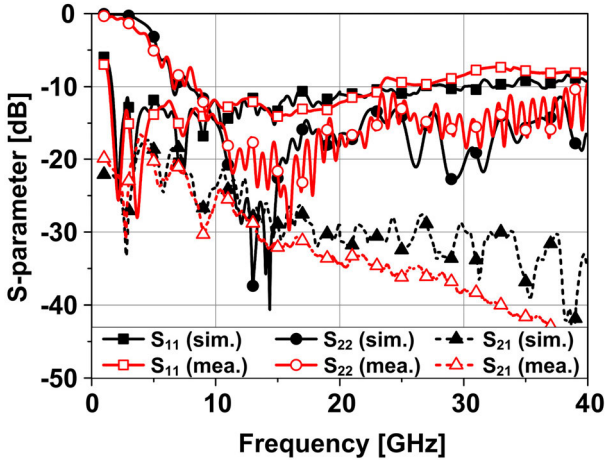

FIGURE 10. Measured and simulated return loss characteristics of the fabricated antenna.

The simulated and measured s-parameter results are compared in Fig. 10. The measured S_{11} is below −10 dB from 1.43 to 23.27 GHz for the lower frequency band and S_{22} is below −10 dB from 8.37 to 39.05 GHz for the upper frequency band. The simulated and measured far-field radiation patterns of the antenna in the xy- and xz-planes for various frequencies are shown in Fig. 11. Nearly uniform patterns

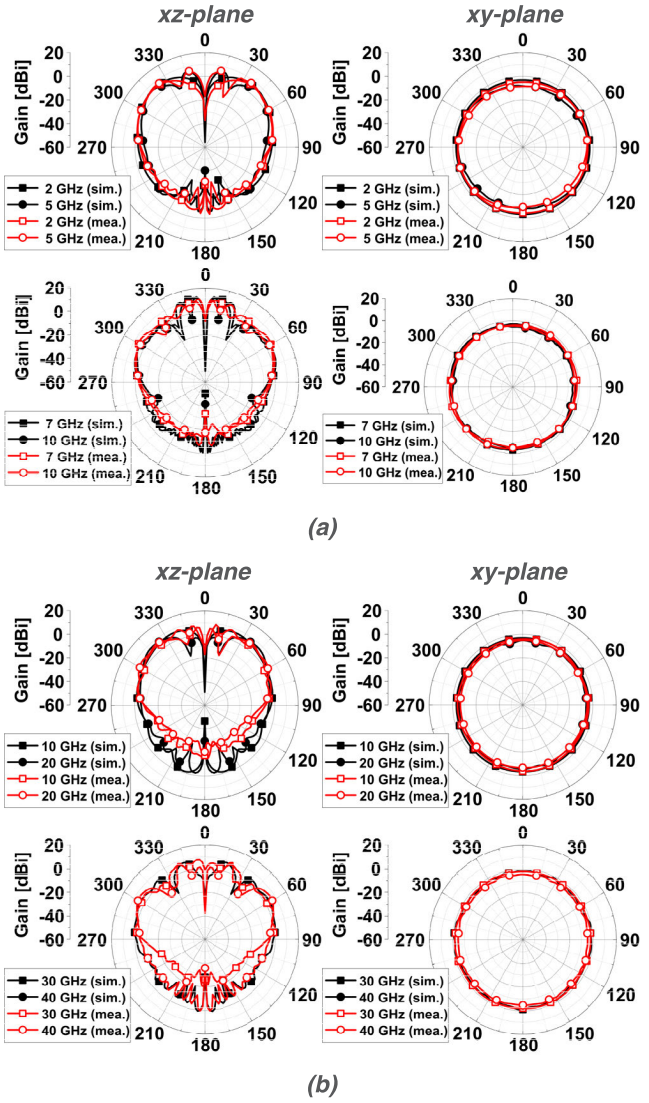

FIGURE 11. Simulated and measured radiation patterns of the proposed antenna in xz- and xy-planes at 2, 5, 7, 10, 20, 30, and 40 GHz: (a) when port1 is excited and (b) when port2 is excited.

are observed in the horizontal plane (the xy-plane), while directional patterns appear in the vertical plane (the xz-plane). The variations of gain in the horizontal plane are less than 3.7 dB for the lower band and less than 2.17 dB for the upper band. The relatively large gain variation for the lower band is due to the vertically induced current on the helical probe and shorting line [25]. Fig. 12 shows the simulated and measured peak gains of the proposed antenna in the xz-plane. The measured peak gain of the proposed antenna varies from 5.78 dBi to 10.71 dBi for the lower band and from 7.89 dBi to 9.07 dBi for the upper band. Note that there are similar discrepancies in the far-field gain due to the high resistance of the conductive spray and surface roughness [18]. The discrepancies are due to the roughness of conductively coated surface and the discontinuity caused by the segmented structure. To overcome these issues, a more precise

TABLE 2. Comparison between proposed and previous related works.

Ref no.	Type	Radiation pattern	Bandwidth	Fractional Bandwidth	Dimension
[7]	Blade	Omnidirectional	20-1200 MHz (VSWR < 2.5)	193.44%	710mm×250mm×50mm $0.047\lambda_L \times 0.017\lambda_L \times 0.003\lambda_L$
[8]	Blade	Omnidirectional	840.5-845 MHz, 1430-1444 MHz, 2408-2440 MHz (RL > 10dB)	0.53%/0.97%/1.32%	117mm×55.7mm×29.6mm $0.328\lambda_L \times 0.156\lambda_L \times 0.083\lambda_L$
[9]	Blade	Omnidirectional	500 MHz-3 GHz (RL > 6dB)	142.86%	500mm×500mm×129mm $0.833\lambda_L \times 0.833\lambda_L \times 0.215\lambda_L$
[10]	Low-profile	Quasi-omnidirectional	807 MHz-835 MHz (RL > 10dB)	3.41%	130.8mm×20mm×10mm $0.352\lambda_L \times 0.054\lambda_L \times 0.027\lambda_L$
[11]	Low-profile	Quasi-omnidirectional	2.39 GHz-2.44 GHz (RL > 10dB)	2.07%	95.5mm×95.5mm×3.5mm $0.761\lambda_L \times 0.761\lambda_L \times 0.027\lambda_L$
[12]	Low-profile	Omnidirectional	1429MHz-1442MHz (VSWR < 2)	0.91%	33.4mm×33.4mm×5mm $0.156\lambda_L \times 0.156\lambda_L \times 0.024\lambda_L$
[13]	Flush-mountable	Omnidirectional	3.4 GHz-5.7 GHz (RL > 10dB)	50.55%	70mm×70mm×10.75mm $0.793\lambda_L \times 0.793\lambda_L \times 0.122\lambda_L$
[14]	Flush-mountable	Near-omnidirectional	2 GHz-6 GHz	100%	570mm×220mm×40mm $3.800\lambda_L \times 1.467\lambda_L \times 0.267\lambda_L$
[15]	Flush-mountable	Quasi-Omnidirectional	1.3 GHz-25.7 GHz (RL > 10dB)	180.74%	224mm×224mm×34mm $0.971\lambda_L \times 0.971\lambda_L \times 0.147\lambda_L$
Proposed	Flush-mountable	Quasi-Omnidirectional	1.43 GHz-39.05GHz (RL >10dB)	185.87%	200mm×200mm×30mm $0.953\lambda_L \times 0.953\lambda_L \times 0.143\lambda_L$

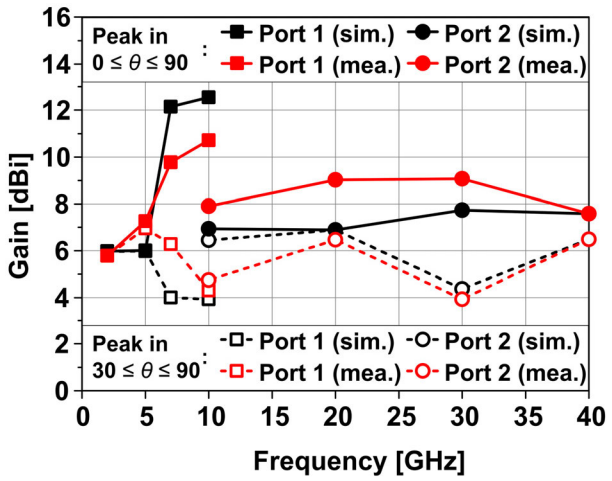

FIGURE 12. Simulated and measured peak gains of the proposed antenna.

manufacturing process (including fine 3D-printing and high quality conductive spray painting) is necessary. The comparison among proposed and previous related works is presented in Table 2 to highlight the merits of the proposed antenna. Indeed, the majority of the studies except [7] and [15] have relatively narrow bandwidth. In [7], wideband operation frequency and omni-directional radiation patterns were obtained. However, the design has a blade type antenna which is not suitable for UAV applications. Since the operating frequency band of the flush-mountable antenna suggested in [15] is not wide enough for fully covering the K-band signals, we are to extend the operating bandwidth in the proposed design. Moreover, the proposed design has the same dimension as that of [15] despite of having an additional small mono-cone antenna.

IV. CONCLUSION

In this paper, a new flush-mountable broadband dual mono-cone antenna for UAV applications was proposed. The proposed antenna consists of four main sections: a small mono-cone, a large mono-cone, an exponentially tapered cavity, and a helical feeding structure. The frequency bandwidth of the mono-cones was enhanced using the exponentially tapered cavity, and the upper frequency band was obtained through the small mono-cone. The helical probe feed (which has little impact on the performance of antenna element) was used to excite the small mono-cone. The proposed antenna was manufactured using 3-D printing technology due to its ability to provide low-cost fabrication and produce lightweight items. The exponentially tapered cavity backed dual mono-cone antenna achieves good quasi-omnidirectionality in broad frequency bands, the lower mono-cone over 1.43-23.27 GHz and the upper mono-cone over 8.37–39.05 GHz, verifying the validity of our approach. Thus, the proposed antenna is a good candidate for aerial applications and can be utilized directly for UAVs.

REFERENCES

[1] K. P. Valavanis, Ed., *Advances in Unmanned Aerial Vehicles: State of the Art and the Road to Autonomy*. New York, NY, USA: Springer-Verlag, 2007.

[2] M. Asadpour, B. V. den Bergh, D. Giustiniano, K. A. Hummel, S. Pollin, and B. Plattner, "Micro aerial vehicle networks: An experimental analysis of challenges and opportunities," *IEEE Commun. Mag.*, vol. 52, no. 7, pp. 141–149, Jul. 2014.

[3] I. Guvenc, F. Koohifar, S. Singh, M. L. Sichitiu, and D. Matolak, "Detection, tracking, and interdiction for amateur drones," *IEEE Commun. Mag.*, vol. 56, no. 4, pp. 75–81, Apr. 2018.

[4] J. Haystead and J. Knowles, "Evolve and adapt: SIGINT for special mission aircraft," *J. Electron. Defense*, vol. 36, no. 2, pp. 20–26, Feb. 2013.

[5] L. L. Horowitz, "Airborne signal intercept for wide-area battlefield surveillance," *Lincoln Lab. J.*, vol. 10, no. 2, pp. 87–98, 1997.

[6] L. Scorrano, F. Trotta, A. Manna, and L. Dinoi, "Dual-polarization DF array for airborne SIGINT in VHF/UHF bands," in *Proc. 11th Eur. Microw. Conf. (EuMC)*, Oct. 2014, pp. 609–612.

[7] M. Nosrati, A. Jafargholi, R. Pazoki, and N. Tavassolian, "Broadband slotted blade dipole antenna for airborne UAV applications," *IEEE Trans. Antennas Propag.*, vol. 66, no. 8, pp. 3857–3864, Aug. 2018.

[8] Y. Cui, P. Luo, Q. Gong, and R. Li, "A compact tri-band horizontally polarized omnidirectional antenna for UAV applications," *IEEE Antennas Wireless Propag. Lett.*, vol. 18, no. 2, pp. 601–605, Apr. 2019.

[9] J. Go, J. Hur, Y. Kay, and H. Choo, "Design of a VHF-UHF band blade antenna for aircraft applications," *J. Korean Inst. Electromagn. Eng. Sci.*, vol. 25, no. 6, pp. 619–627, Jun. 2014.

[10] Z.-Q. Liu, Y.-S. Zhang, Z. Qian, Z. P. Han, and W. Ni, "A novel broad beamwidth conformal antenna on unmanned aerial vehicle," *IEEE Antennas Wireless Propag. Lett.*, vol. 11, pp. 196–199, 2012.

[11] L. Sun, B. Sun, J. Yuan, W. Tang, and H. Wu, "Low-profile, quasi-omnidirectional substrate integrated waveguide (SIW) multihorn antenna," *IEEE Antennas Wireless Propag. Lett.*, vol. 15, pp. 818–821, 2016.

[12] D. Wu, X. Chen, L. Yang, G. Fu, and X. Shi, "Compact and low-profile omnidirectional circularly polarized antenna with four coupling arcs for UAV applications," *IEEE Antennas Wireless Propag. Lett.*, vol. 16, pp. 2919–2922, 2017.

[13] L. Rufail and J.-J. Laurin, "Aircraft cavity-backed nonprotruding wideband antenna," *IEEE Antennas Wireless Propag. Lett.*, vol. 11, pp. 1108–1111, Sep. 2012.

[14] G. Artner, R. Langwieser, and C. F. Mecklenbräuker, "Concealed CFRP vehicle chassis antenna cavity," *IEEE Antennas Wireless Propag. Lett.*, vol. 16, pp. 1415–1418, 2017.

[15] S. Lee, G. Jeoung, and J. Choi, "Three-dimensional-printed tapered cavity-backed flush-mountable wideband antenna for UAV," *Microw. Opt. Technol. Lett.*, vol. 59, no. 12, pp. 2975–2981, 2017.

[16] K. V. Hoel, S. Kristoffersen, J. Moen, G. Holm, and T. S. Lande, "Characterization of a 3D printed wideband waveguide and horn antenna structure embedded in a UAV wing," in *Proc. 10th Eur. Conf. Antennas Propag. (EuCAP)*, Davos, Switzerland, Apr. 2016, pp. 1–4.

[17] B. Rohrdantz, C. Rave, and A. F. Jacob, "3D-printed low-cost, low-loss microwave components up to 40 GHz," in *IEEE MTT-S Int. Microw. Symp. Dig.*, San Francisco, CA, USA, May 2016, pp. 1–3.

[18] J. Tak, D.-G. Kang, and J. Choi, "A lightweight waveguide horn antenna made via 3D printing and conductive spray coating," *Microw. Opt. Technol. Lett.*, vol. 59, no. 3, pp. 727–729, 2017.

[19] J. Zhao, D. Psychoudakis, C.-C. Chen, and J. L. Volakis, "Design optimization of a low-profile UWB body-of-revolution monopole antenna," *IEEE Trans. Antennas Propag.*, vol. 60, no. 12, pp. 5578–5586, Dec. 2012.

[20] K. Y. Mok, Y. C. Rhee, and J. H. Yoon, "Design of a pot-shaped monopole antenna with dual band notched characteristics for UWB application," *J. Electromagn. Eng. Sci.*, vol. 17, no. 1, pp. 44–49, 2017.

[21] *ANSYS HFSS*, Version 2015.2, ANSYS Corp., Pittsburgh, PA, USA, 2017.

[22] R. C. Johnson and H. Jasik, *Antenna Engineering Handbook*, 2nd ed. New York, NY, USA: McGraw-Hill, 1984.

[23] J. L. McDonald and D. S. Filipovic, "A monocone-bicone collinear array," *IEEE Trans. Antennas Propag.*, vol. 58, no. 12, pp. 3905–3912, Dec. 2010.

[24] D. D. Button, W. D. Wyatt, and J. F. McGrath, "Stacked biconical omnidirectional antenna," U.S. Patent 5 534 880, Jul. 9, 1996.

[25] S. M. A. M. H. Abadi and N. Behdad, "An electrically small, vertically polarized ultrawideband antenna with monopole-like radiation characteristics," *IEEE Antennas Wireless Propag. Lett.*, vol. 13, pp. 742–745, 2014.

[26] K.-S. Keum, Y.-M. Park, and J.-H. Choi, "A low-profile wideband monocone antenna using bent shorting strips," *Appl. Sci.*, vol. 9, no. 9, p. 1896, 2019.

[27] W. Jeong, J. Tak, and J. Choi, "A low-profile IR-UWB antenna with ring patch for WBAN applications," *IEEE Antennas Wireless Propag. Lett.*, vol. 14, pp. 1447–1450, 2015.

SEONGKYU LEE received the B.S. degree in electronic engineering from Hanyang University, Seoul, South Korea, in 2013, where he is currently pursuing the combined master's and Ph.D. degrees with the Department of Electronics and Computer Engineering. His current research interests include RF components including antenna design, wireless communication systems, wireless power transferring, and wireless body area networks.

SUNRYUL KIM received the B.S. degree in electronic engineering from Hanyang University, Seoul, South Korea, in 2015, where he is currently pursuing the M.S. degree with the Department of Electronics and Computer Engineering. His current research interests include multiband antennas and the miniaturization of antennas.

YOUNGMI PARK received the B.S. and M.S. degrees in computer science from Chungnam National University, Daejeon, South Korea, in 1991 and 2005, respectively. She is currently with the Agency for Defence Development, Daejeon. Her current research interests include the area of radar signal processing, electronic warfare signal processing, and direction finding systems.

JAEHOON CHOI received the B.S. degree from Hanyang University, South Korea, and the M.S. and Ph.D. degrees from The Ohio State University, Columbus, OH, USA, in 1980, 1986, and 1989, respectively. From 1989 to 1991, he was a Research Analyst with the Telecommunication Research Center, Arizona State University, Tempe, AZ, USA. From 1991 to 1995, he was with Korea Telecom, as a Team Leader of the Satellite Communication Division. Since 1995, he has been a Professor with the Department of Electronic Engineering, Hanyang University, South Korea. He has published more than 200 peer-reviewed journal articles and contributed to numerous conference proceedings. He holds more than 100 domestic and international patents. His current research interests include antennas, microwave circuit design, and EMC, especially the design of compact, multiband antennas for mobile wireless communication, and military applications.